GEOPHYSICS, VOL. 52, NO. 12 (DECEMBER 1987); P. 1697–1707, 12 FIGS.

Natural-field and very low-frequency tipper profile interpretation of contacts

Victor F. Labson* and Alex Becker‡

ABSTRACT

Anomalous vertical magnetic field (tipper) profiles acquired using natural or very low-frequency (VLF) radio transmitter sources can be interpreted simply and rapidly for a number of geologic settings. The relations between computed numerical models, and outcropping dipping and buried vertical contacts are presented here in a series of interpretation charts. Use of the tipper phase in the analysis minimizes the effect of transmitter azimuth in the VLF case.

Two examples illustrate the application to field data. An audiofrequency natural-field tipper profile over a conductive bed in a north-central Washington State metasedimentary sequence demonstrates the interpretation procedure for a dipping contact. VLF profiles over covered basement faults in Ontario demonstrate the application for a buried vertical contact. In both cases the quick results are in agreement with the much more laborious trial-and-error matching to two-dimensional models.

INTRODUCTION

An efficient geophysical method of mapping lateral subsurface discontinuities of electrical conductivity is based on the detection and measurement of the associated anomalous vertical magnetic fields (Ward, 1959; Labson et al., 1985). In such cases the horizontally polarized primary fields from magnetic sources for the electromagnetic (EM) induction process can be either natural or manmade (e.g., VLF transmitters) and can cover a frequency range exceeding 10^{-3} Hz to 60 kHz. The anomalous vertical magnetic field arises when the source field propagates in the transverse electric (TE) mode, in which the electric-field vector is parallel to the strike of the subsurface electrical conductivity discontinuity and the primary magnetic field is perpendicular to strike.

In geophysical studies using natural magnetic fields, the objective is the ratio of the observed vertical component to the total horizontal component measured perpendicular to the strike of the conductivity anomaly. Because these two orthogonal components of the magnetic field differ in phase, their ratio is expressed as a complex number commonly referred to as the "tipper" (Vozoff, 1972). For natural fields, this quantity is a stable indicator of subsurface conductors because the observed time-averaged values do not depend upon the direction of propagation of the primary source fields (Labson et al., 1985). In the case of manmade VLF signals, the measurement is also stable although the measured horizontal magnetic-field component will be polarized in the direction perpendicular to the azimuth of the transmitter rather than to the subsurface electrical anomaly. In this case the observed ratio can depend upon the orientation of the transmitter with respect to the conductivity anomaly.

The vertical magnetic field observed at the surface is a direct result of the associated induction process which modifies the distribution of electric current in and near the anomalous body. The geometrical parameters for this EM induction problem preclude a closed-form analytical solution; thus the expected vertical magnetic fields over any given geologic model must be computed numerically. The field data therefore have proven difficult to interpret. In fact, the cost of data interpretation can often exceed the cost of data acquisition.

Tipper data may be interpreted in different ways. One method, which is qualitative, involves the application of numerical operators to the survey results. An example of this technique is the spatial filtering of survey data first proposed by Fraser (1969) and more recently discussed by Karous and Hjelt (1983). The numerical upward and downward continuation procedures outlined by Watts (1975) fall into the same category. These qualitative methods reduce the apparent complexity of the survey data and are useful for distinguishing

Presented at the 55th Annual International Meeting, Society of Exploration Geophysicists, Washington, D.C. Manuscript received by the Editor October 27, 1986; revised manuscript received June 4, 1987.
*U.S. Geological Survey, Box 25046, MS 964, Denver Federal Center, Denver, CO 80225.
‡Engineering Geoscience, University of California, 414 Hearst Mining Building, Berkeley, CA 94720.

good conductors from poor conductors, and shallow conductors from deep conductors. These methods provide little assistance, however, in determining the electrical parameters of the subsurface structure quantitatively. In this respect, suites of model curves such as those compiled by Vozoff (1971), Kaikkonen (1979), and Olsson (1980) for a conductive dike or those presented by Telford et al. (1977) for a buried vertical contact are more useful since they provide a means for testing and interpretation of a hypothesis by a comparison between the field data set and the model data set. A complete interpretation of the field data can only be made by using a combination of numerical modeling and iterative data inversion. One can either use a simple trial-and-error approach (Morrison et al., 1979) or an automated procedure (Jupp and Vozoff, 1977). In either case this technique requires considerable computation time and can be prohibitively expensive.

We propose a simple method of interpreting tipper measurements acquired over two elementary but very common geologic features, an outcropping contact with a variable dip and a vertical contact covered by an overburden layer. Using an approach similar to that suggested by Saydam (1981) for determining the depth and conductance of a buried dike, with the aid of specialized charts one can readily determine the electrical properties of these subsurface features from the characteristics of the observed data profiles. This procedure for interpreting field data requires only measurements at a single frequency and can be readily carried out in the field.

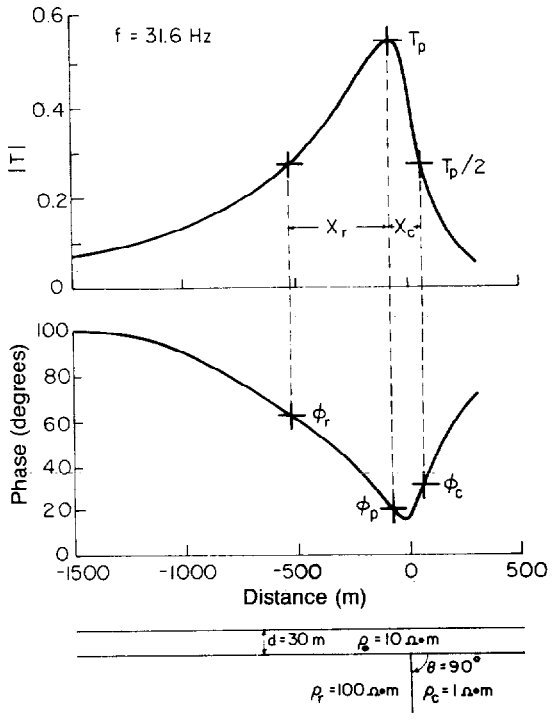

FIG. 1. Numerical solution of a vertical contact of a 100 Ω · m resistive and 1 Ω · m conductive formation under a 30 m thick, 10 Ω · m overburden at 31.6 Hz. Tipper magnitude and phase profiles show parameters required for interpretation.

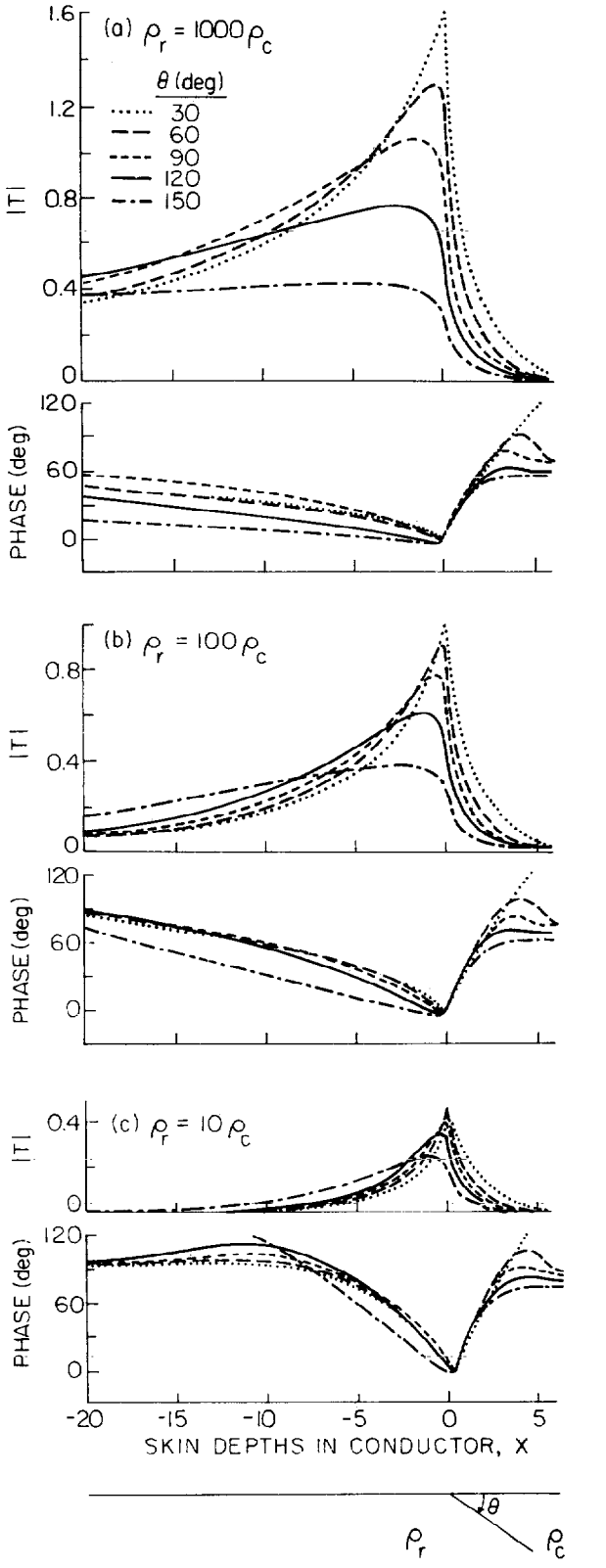

FIG. 2. Numerical solutions of dipping contacts with resistivity ratios of (a) 1000:1; (b) 100:1; and (c) 10:1. Tipper magnitude $|T|$ and phase for dips of 30, 60, 90, 120, and 150 degrees. Horizontal scale is in units of skin depth in the conductive medium.

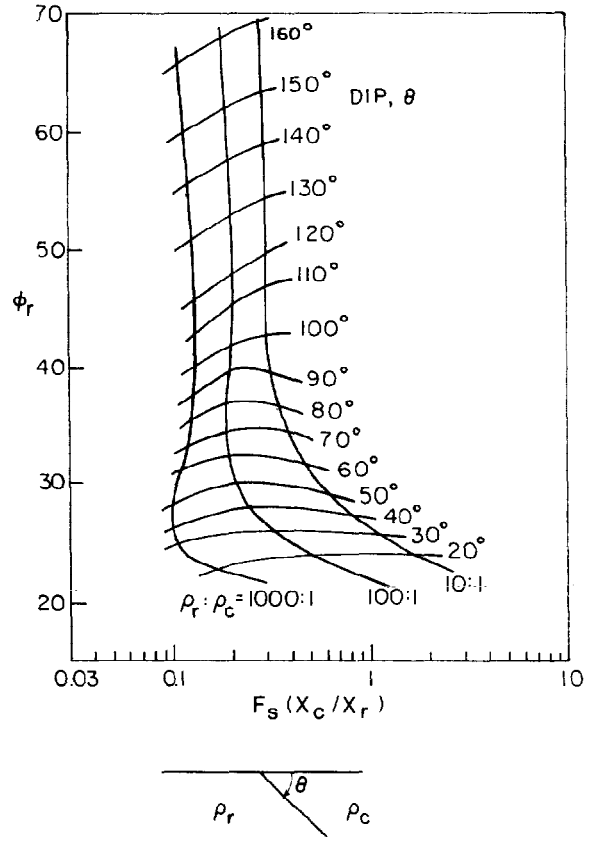

FIG. 3. Dipping contact: relation of dip Θ and resistivity contrast $\rho_r:\rho_c$ to the ratio of half-widths $F_s = x_c/x_r$ and the phase at the resistive half-width point ϕ_r.

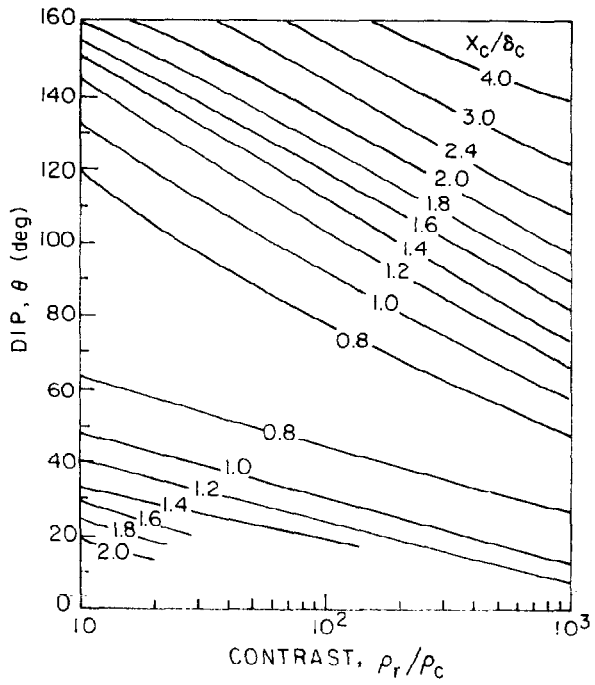

FIG. 4. Dipping contact: relation of the conductive half-width in units of skin depths in the conductor x_c/δ_c to dip and resistivity contrast.

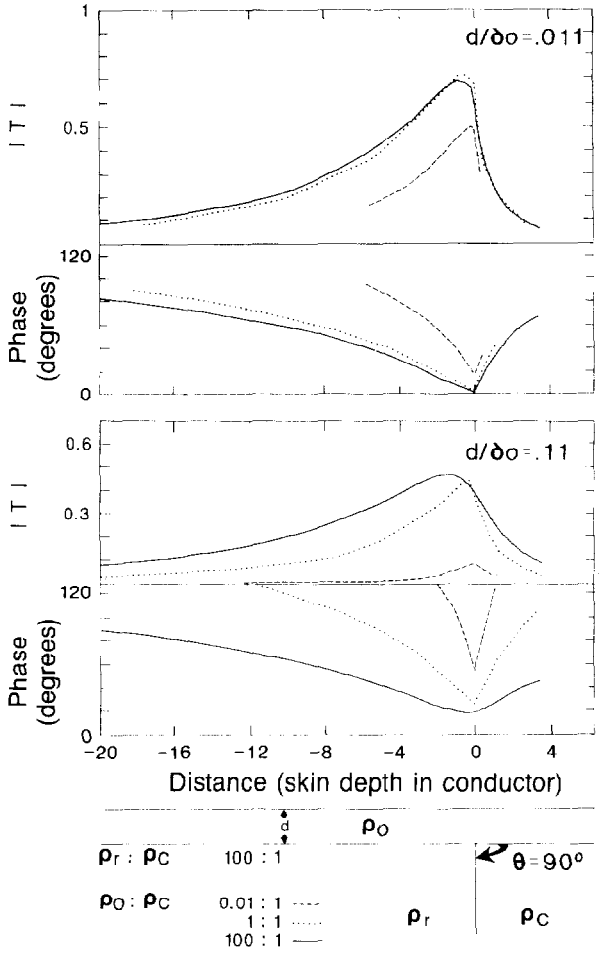

FIG. 5. Tipper magnitude and phase profiles from numerical solution of a vertical contact with a resistivity contrast $\rho_r:\rho_c$ of 100:1. Overburden-to-conductor resistivity contrast $\rho_0:\rho_c$ of 0.01:1, 1:1, and 100:1. Overburden thicknesses d/δ_0 of 0.011 and 0.11 skin depths.

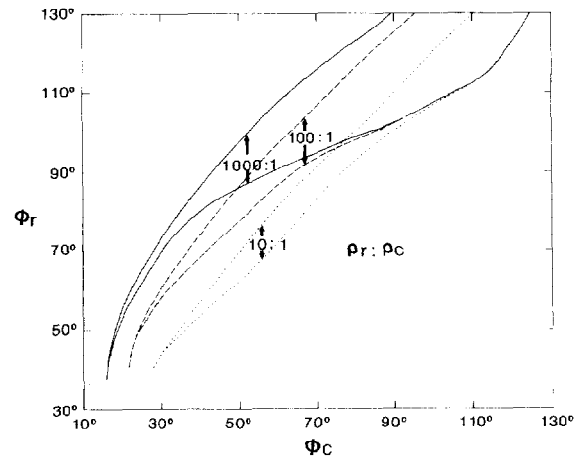

FIG. 6. Vertical contact: relation of the phases at resistive and conductive half-width points ϕ_r and ϕ_c to resistivity contrast $\rho_r:\rho_c$.

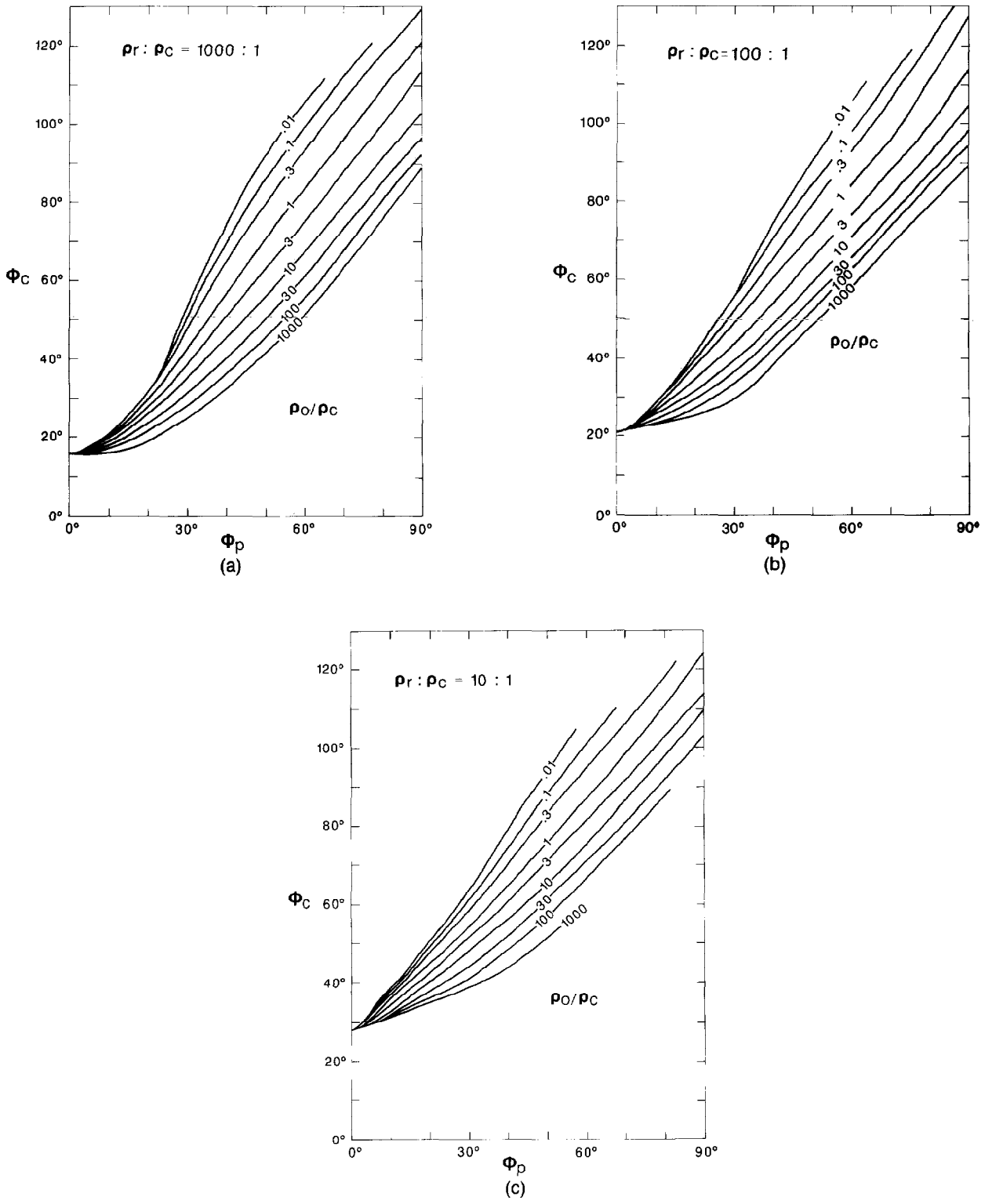

FIG. 7. Vertical contact: relation of phase at the conductive half-width point θ_c and peak tipper magnitude's phase θ_p to the resistivity contrast of the overburden to conductor ρ_0/ρ_c for (a) $\rho_r:\rho_c = 1000:1$; (b) $\rho_r:\rho_c = 100:1$; and (c) $\rho_r:\rho_c = 10:1$.

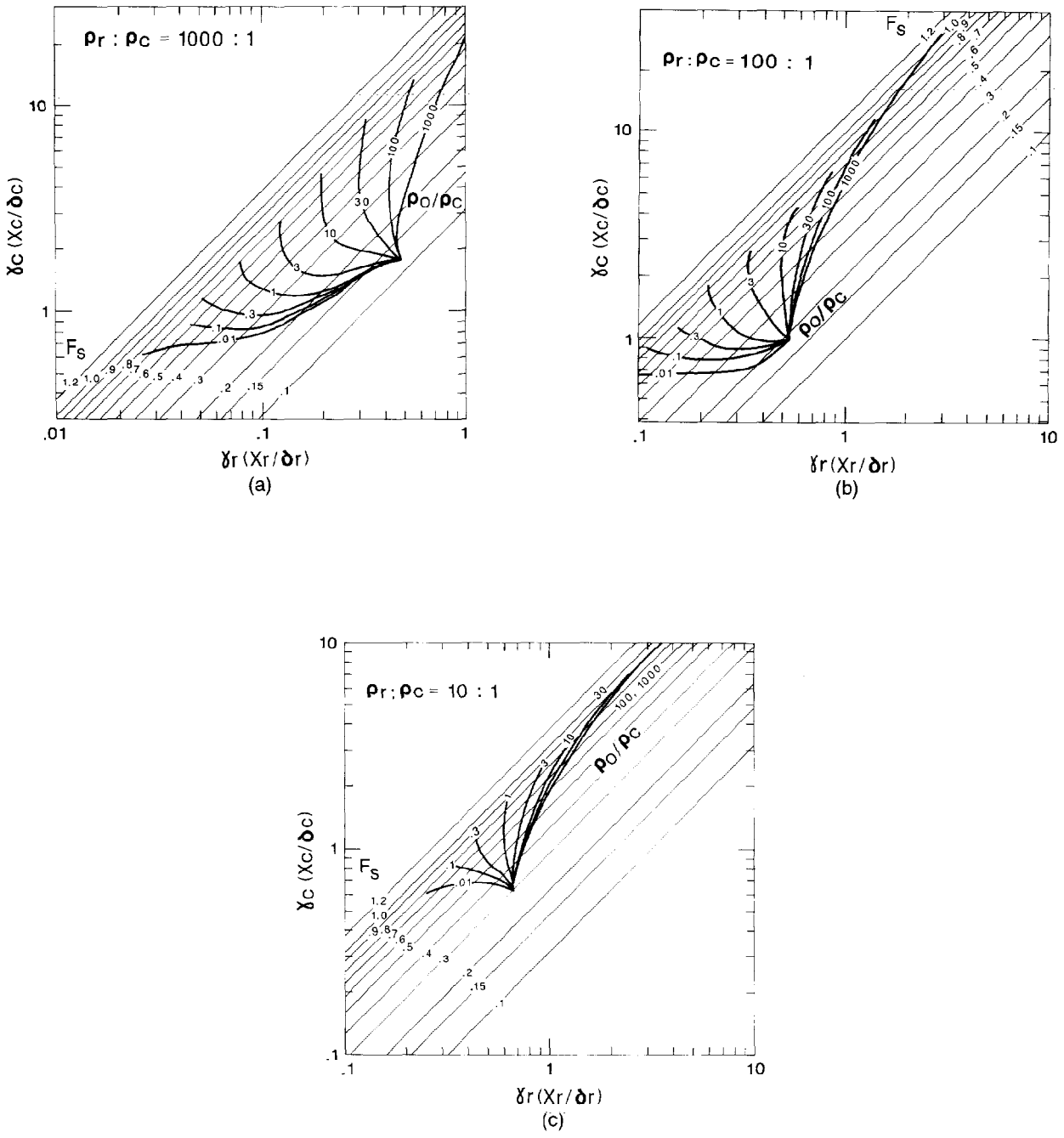

FIG. 8. Vertical contact: relation of the ratio of half-widths F_s and resistivity contrast of overburden to conductor ρ_0/ρ_c to the conductive half-widths in units of skin depth in the conductor γ_c and the resistive half-width in units of skin depth in the resistor γ_r for (a) $\rho_r : \rho_c = 1000 : 1$; (b) $\rho_r : \rho_c = 100 : 1$; and (c) $\rho_r : \rho_c = 10 : 1$.

The observed quantities required for interpretation are the peak tipper magnitude T_p; its phase ϕ_p; the phases ϕ_c and ϕ_r, at the two points where the tipper magnitude falls to one-half of its maximum value; and x_c and x_r, the distances from the peak tipper magnitude to the half-maximum points. These characteristic points and values are identified in Figure 1, which shows the computed profile for a buried vertical contact.

CHARTS FOR A DIPPING CONTACT

The basic model data for constructing the required interpretation charts are derived from two-dimensional (2-D) numerical solutions to the TE induction problem. The computations were done in a right-handed coordinate system with the vertical direction positive upward and an $e^{i\omega t}$ time dependence. Both a transmission-line analogy (Madden, 1972) and a finite-element method (Ryu, 1971; Morrison et al., 1979) were used to perform the required calculations. Differences between the two methods were kept to less than 5 percent. Figure 2 shows profiles, over a contact extending to the surface, of tipper magnitude and phase as functions of a dimensionless distance expressed in terms of the skin depth in the conductive medium. The data shown cover a wide range of contact parameters, spanning five values for the dip and three values for the resistivity contrast. The position of the minimum tipper phase is nearly coincident with the location of the contact. In most cases the asymmetry of the tipper profile clearly identifies the conductive side of the contact which is associated with the steep side of the anomaly. In cases of very shallow dip and low contrast, however, other means must be used to identify the conductive side.

Two interpretation charts are needed to interpret the field data observed over a dipping geologic contact that extends to the surface. The first chart (Figure 3) is needed to determine the dip and the resistivity contrast for the contact. The observed anomaly characteristics used here are ϕ_r, the tipper phase at the half-maximum point on the resistive side, and F_s, the ratio of the conductive to the resistive half-width (x_c/x_r). Once the dip and the resistivity contrast are known, the dimensionless distance γ_c between the tipper peak and its half-maximum value on the conductive side of the contact may be determined. This information could be obtained from Figure 2, but it can be obtained more easily from the second chart (Figure 4). The resistivity of the conductive side of the contact is then given by

$$\rho_c = \left[(x_c \sqrt{f})/(503\ \gamma_c) \right]^2, \qquad (1)$$

where

ρ_c = resistivity ($\Omega \cdot$ m) on the conductive side,
x_c = half-width (meters) on the conductive side,
γ_c = half-width (skin depths, x_c/δ_c) from Figure 4,
δ_c = 503 $(\rho_c/f)^{1/2}$ skin depth,

and

f = frequency (hertz) at which the data were acquired.

The interpretation is completed by determining the resistivity (ρ_r) on the resistive side of the contact from the contrast value (ρ_r/ρ_c) obtained previously.

Even when the surficial contact cannot be seen, it can be identified directly from the field data by observing that the phase associated with the peak tipper magnitude value is zero. Of all the 2-D structures examined in this study, the surficial contact is the only one that exhibits this particular characteristic. In practice, it appears that this model can be used to interpret all field data where the phase angle associated with the peak tipper magnitude is less than 10 degrees.

Charts for a buried vertical contact

Although we have not been able to create interpretation charts for the general case of a buried dipping contact, the common occurrence of buried vertical contacts merits some special attention. This case is often identified from geologic considerations or ancillary geophysical data. It differs from the contact at the surface in that the phase angle associated with peak tipper magnitude is no longer zero, but varies with overburden thickness d and resistivity ρ_0. In general the presence of the overburden alters the observed anomaly which now depends upon overburden thickness and resistivity as well as on the electrical parameters of the contact. Typical numerical data for this case appear in Figure 5 where profiles of tipper magnitude and phase are shown for a contact with a resistivity contrast ρ_r/ρ_c of 100. The data are presented as a function of distance normalized to the skin depth in the more conductive contact formation in a manner similar to that used in preparing Figure 2. In this case, however, we have also considered two values of overburden thickness (0.011 and 0.11 skin depths) and overburden resistivities of 0.01, 1, and 100 times the conductive formation's resistivity. Clearly, even a small amount of overburden attenuates and changes the form of the observed tipper profile.

Because two additional overburden parameters ρ_0 and d must be evaluated, our procedure for interpreting data acquired over a buried vertical contact requires more charts than in the simpler case of a contact extending to the surface. The procedure still involves the identification of the conductive and resistive sides by inspection and the use of the characteristic distances x_c and x_r, their ratio F_s, and the tipper phases ϕ_c and ϕ_r at the half-maximum points. In addition, we require ϕ_p, the tipper phase associated with the peak tipper magnitude. As before, the position of the minimum value of tipper phase corresponds to the contact position.

The interpretation process starts with the determination of the resistivity contrast $\rho_r : \rho_c$ between the two contact formations. This contrast is found using the chart shown in Figure 6, where the input consists of the two characteristic values of tipper phase ϕ_c and ϕ_r. In some regions of the chart, particularly in the zone corresponding to high characteristic phase values, it is not possible to obtain a unique value for the resistivity contrast due to the effect of the overburden resistivity. Experience shows, however, that one can proceed with the interpretation by arbitrarily choosing any resistivity contrast within the overlapping range. Apart from possibly causing a large error in the estimate for the resistivity of the resistive formation ρ_r, no other serious inaccuracies result from this ambiguity which arises when the overburden is thick.

We next establish the resistivity contrast between the conductive formation and the overburden. The tipper phase is again used, after having chosen the appropriate chart in Figure 7 according to the resistivity contrast between the two bedrock formations in contact. Here the characteristic phase on the conductive side ϕ_c and the phase associated with the peak tipper magnitude ϕ_p are used to determine the resistivity contrast ρ_0/ρ_c.

At this point we can find the resistivities of the two bedrock formations that form the contact. Using the bedrock resistivity contrast $\rho_r:\rho_c$, one chooses the appropriate chart in Figure 8. The intersection of the parametric curves for the half-width ratio F_s and the ratio of the resistivities of the overburden and conductive formation ρ_0/ρ_c identifies the normalized half-width distances γ_c and γ_r. As in the case of the dipping contact at the surface, one obtains the resistivity of the conductive formation from equation (1) by inserting the observed value of x_c and the value of γ_c determined from Figure 8. The two other resistivities needed to complete the problem are determined from the resistivity contrasts ρ_r/ρ_c and ρ_0/ρ_c established in the first part of the interpretation procedure.

The interpretation can now be completed by determining the depth of overburden from the appropriate chart in Figure 9. Here one reads in the tipper phase observed at the point of peak tipper magnitude ϕ_p and the overburden-conductor resistivity contrast ρ_0/ρ_c obtained from Figure 7. The value of γ_0, the dimensionless overburden depth, is then found along the ordinate. The actual overburden thickness is

$$d = 503\ \gamma_0(\rho_0/f)^{1/2}, \tag{2}$$

where

d = overburden thickness in m,
γ_0 = dimensionless thickness,
ρ_0 = overburden resistivity in $\Omega \cdot$ m,

and

f = frequency at which measurements are made.

Because the proposed interpretation method relies solely on the phase relations and the shape of the profile, it can be used to interpret fixed-transmitter VLF data, regardless of the orientation of the transmitter in relation to the contact. The dependence of the field quantities on the transmitter azimuth explains this relationship. There are no secondary vertical or

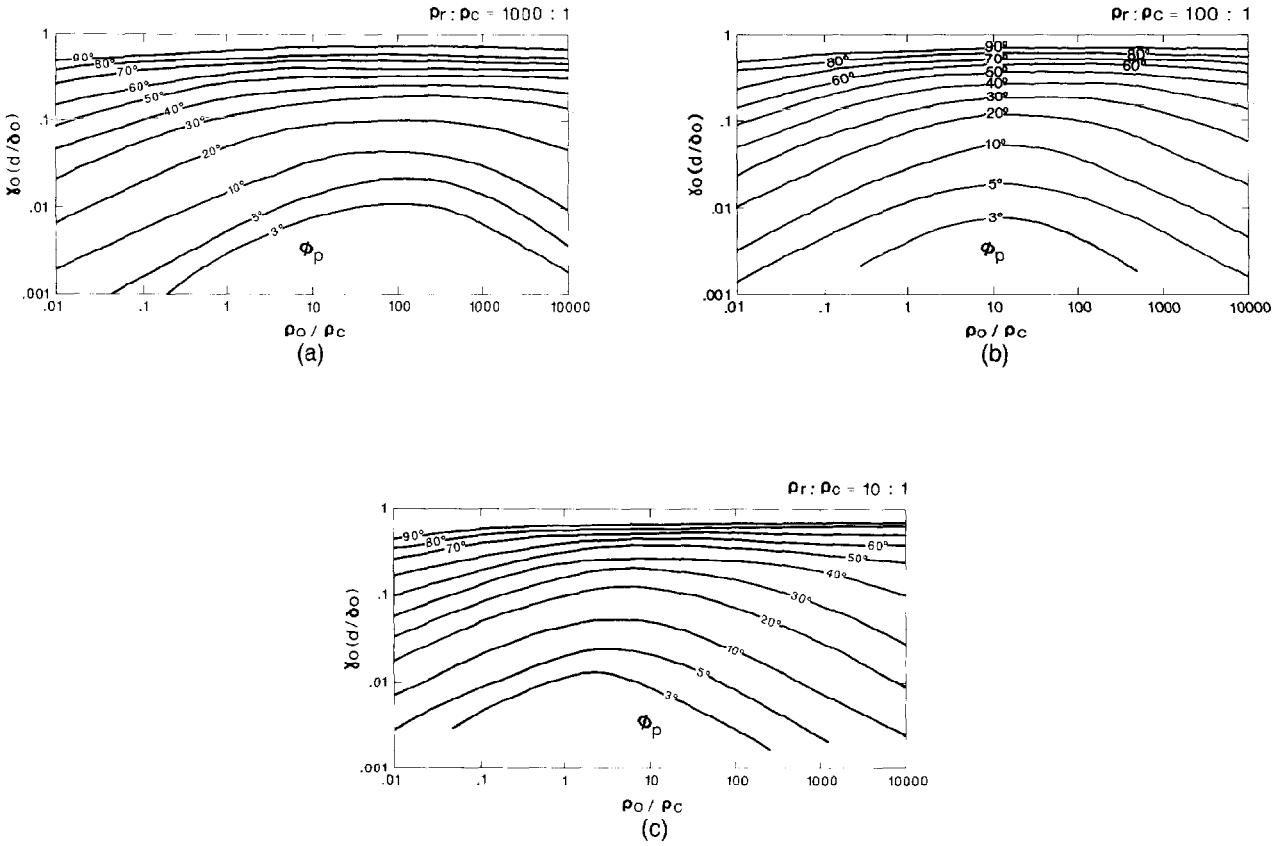

FIG. 9. Vertical contact: relation of the resistivity contrast of overburden to conductor $\rho_0:\rho_c$ and phase of the peak tipper ϕ_p to the overburden thickness in units of skin depth in the overburden γ_0 for (a) $\rho_r:\rho_c = 1000:1$; (b) $\rho_r:\rho_c = 100:1$; and (c) $\rho_r:\rho_c = 10:1$.

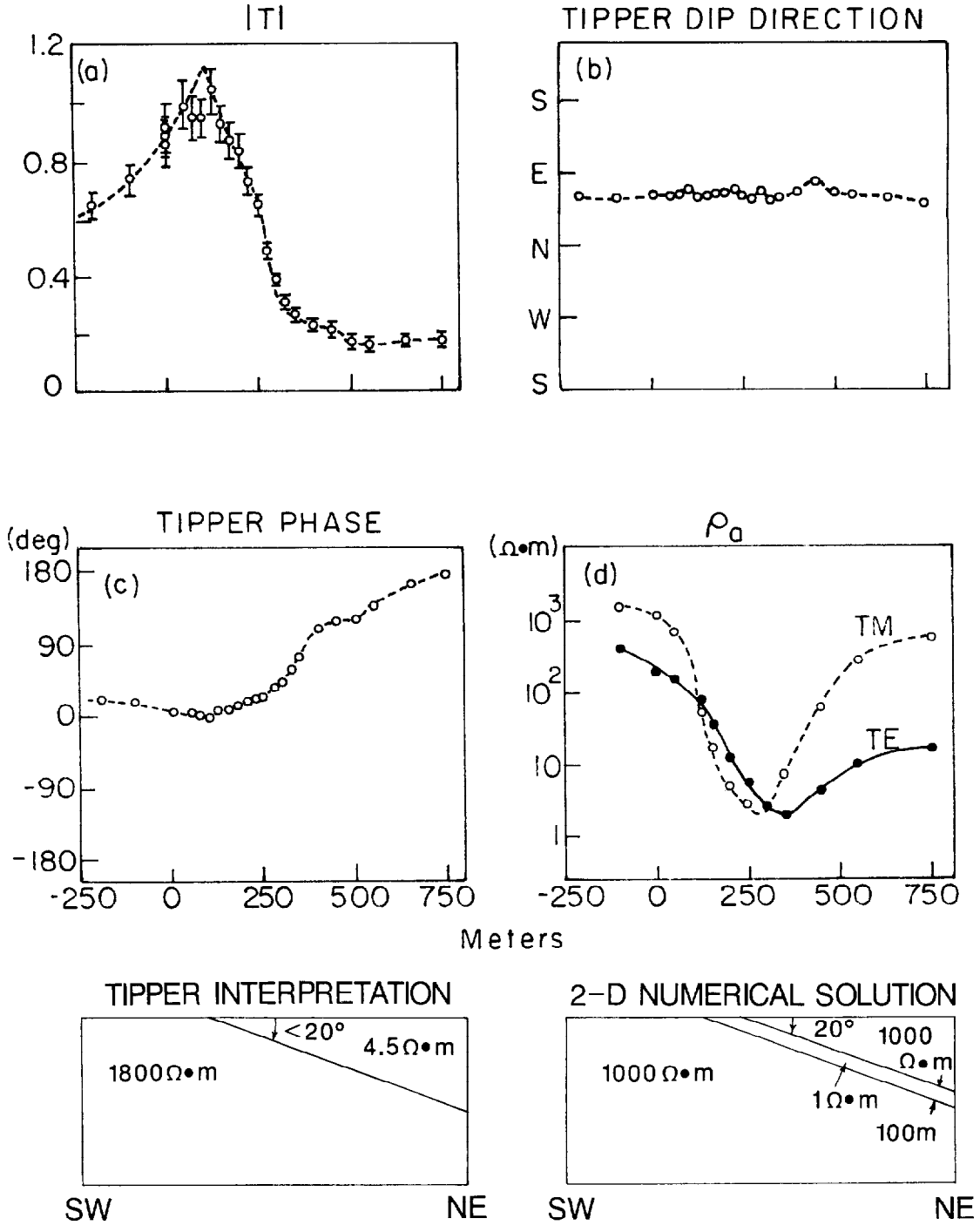

FIG. 10. Dipping contact example. North-central Washington profiles at 100 Hz; (a) tipper magnitude, (b) tipper dip direction, (c) tipper phase, and (d) apparent resistivity. Tipper dip direction was chosen so that tilt is positive toward the conductor. Bars are 50 percent confidence level (not shown where smaller than the symbol). Tipper interpretation is from the interpretation charts in Figures 3 and 4; MT interpretation is from the iterative forward solution.

horizontal magnetic fields associated with a primary horizontal magnetic field parallel to the strike of the conductor. For scalar measurements, the amplitudes of the vertical field and (to the first order) the tipper are functions of the cosine of the angle between the strike of the contact and the azimuth to the transmitter (Paterson and Ronka, 1971). This relation can be written as

$$T_{\text{obs}} = H_z \cos(\theta_{TX}) \Big/ \left[H^p + H_x^s \cos^2(\theta_{TX}) \right], \qquad (3)$$

where

T_{obs} = observed tipper,
θ_{TX} = angle between the contact's strike and the azimuth to the transmitter,
H_z = vertical magnetic field that would be observed for $\theta_{TX} = 0$,
H_x^s = secondary horizontal magnetic field perpendicular to strike that would be observed for $\theta_{TX} = 0$,

and

H^p = primary horizontal field.

Because the secondary horizontal magnetic field is in general small compared to the primary horizontal field, the observed tipper is (to the first order) equal to the cosine of θ_{TX} times the actual tipper. The phase and shape of the profile are changed only by the reduction of the secondary horizontal field. Consequently, an interpretation based on the phase and shape is relatively unaffected by the orientation of the transmitter.

Furthermore, note that the magnitude and phase of the tipper are intimately related (Labson et al., 1985) to the field quantities such as tilt angle and ellipticity measured by many VLF detectors now in use. One should ensure that the instrument employed is correctly calibrated. Calibration that is consistent with the interpretation aids presented here will yield positive tilt angles when the contact is traversed from the resistive side to the conductive side. In this case the minor axis of the polarization ellipse of the magnetic field always points to the conductor.

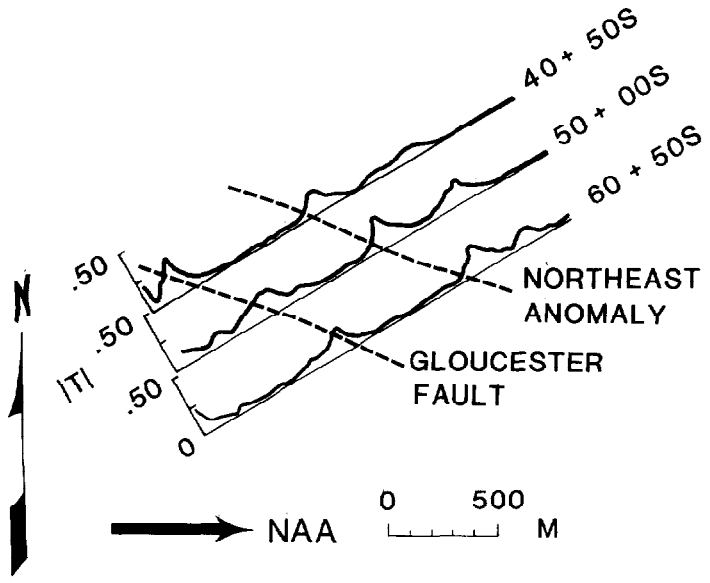

	GLOUCESTER FAULT				NORTHEAST ANOMALY			
Line	ρ_c (Ω•m)	ρ_r (Ω•m)	ρ_o (Ω•m)	d (m)	ρ_c (Ω•m)	ρ_r (Ω•m)	ρ_o (Ω•m)	d (m)
40+50S	144	1440	43	0.2	204	2040	41	4
50+00S	262	2620	26	4	94	940	65	3
60+50S	224	2240	67	9	356	3560	4	0.2

FIG. 11. Ontario VLF tipper magnitude $|T|$ over the Gloucester fault and northeast anomaly, adapted from Telford et al. (1977), with results of the interpretation.

The tipper magnitude $|T|$ and phase ϕ may be computed from the tilt angle ψ in degrees and the ellipticity ε by

$$|T| = \left[(\tan^2 \psi + \varepsilon^2)/(1 + \varepsilon^2 \tan^2 \psi)\right]^{1/2} \quad (4)$$

and

$$\phi = \arctan \left\{\left[\varepsilon(1 + \tan^2 \psi)\right]/\left[(1 - \varepsilon^2) \tan \psi\right]\right\}. \quad (5)$$

FIELD EXAMPLES

Dipping contact

The data set for a possible dipping contact was acquired over a metasedimentary sequence in north-central Washington State. The measurements include the tipper and the two principal magnetotelluric (MT) impedances in the frequency range of 1–500 Hz. Figure 10 illustrates the data profile at 100 Hz. The tipper values have been rotated to the direction of the tipper dip, the direction in which the vertical and horizontal magnetic fields are most coherent (Vozoff, 1972). A visual inspection of the tipper profile at this frequency suggests that it can be interpreted as a geologic contact. The tipper phase at the position of peak tipper magnitude is only 1 degree, indicating that the effect of the overburden layer is negligible; thus the charts for the contact at the surface in Figures 3 and 4 can be used. The profile data in Figure 10 give a conductive half-width of 150 m, a half-width ratio F_s of 0.4, and a phase at the resistive half-width point ϕ_r of 22 degrees. Using this information on the chart in Figure 3, we establish that the dip at the contact is somewhat less than 20 degrees to the northeast and that the resistivity contrast at the contact is about 400. Using these two parameter values as input to the chart in Figure 4, we readily find that the characteristic anomaly half-width on the conductive side x_c corresponds to 1.4 skin depths in the conductive formation. This distance on the anomaly profile equals 150 m; thus equation (1) assigns a resistivity of 4.5 $\Omega \cdot$ m to the conductive side of the contact and a resistivity of 1800 $\Omega \cdot$ m to the resistive side of the contact.

This geologic feature has not been drilled, thus we have no direct verification of the above interpretation. Nevertheless, if one attempts a trial-and-error interpretation of all available data and pays attention to securing a good fit to the MT apparent-resistivity information, the data are best interpreted as arising from a dipping conductive bed. This interpretation is also shown in Figure 10, which indicates a 20 degree dip and a 100 m thickness for the mapped bed. The resistivity of the bed is about 1 $\Omega \cdot$ m, and the resistivity of the host rock is about 1000 $\Omega \cdot$ m. From high-frequency data, the overburden appears to be less than 5 m thick and has a resistivity of about 40 $\Omega \cdot$ m. At 100 Hz this overburden represents less than 0.02 skin depths and has virtually no effect on the response.

Although the observed anomaly is most probably caused by the flatly dipping bed rather than a simple contact, the graphic interpretation method yields satisfactory estimates for the dip and formation resistivities because the upper contact between the conductive and resistive formations gives a small response, illustrated in Figure 2 by the profiles with large dips. If the dip were steeper, the interpretation of the data as representing a simple contact would prove unreliable. In that case a dike model should be used.

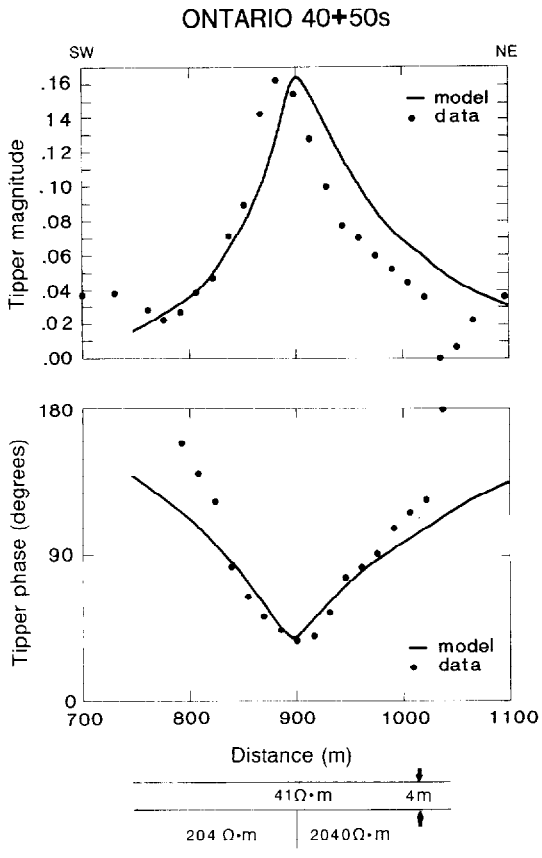

FIG. 12. Ontario VLF profile 40 + 50S over the northeast anomaly: tipper magnitude (top) and phase (bottom) of data (dots) and model of Figure 11 results (line).

Buried vertical contact

Data that can be related to a buried vertical contact were acquired by Telford et al. (1977) in the course of a VLF survey of the Gloucester fault in Ontario, Canada. Surface geology and a gravity survey (Paul and Goodacre, 1984) show that this southeasterly trending feature forms a nearly vertical dividing plane between the resistive dolomitic March sandstone and a conductive shale. Part of the observed tipper data, which were calculated from measurements of tilt angle and ellipticity, are shown in Figure 11. The angle between the trend of the fault and the azimuth to the 17.8 kHz NAA transmitter (Cutler, ME) was approximately 45 degrees. Two sizable anomalies are seen on each profile. The southwestern anomaly is the Gloucester fault; the northeastern feature was not indicated by the surface geology.

The three profiles shown were interpreted using the characteristic features of each anomaly and the appropriate charts in Figures 6–9. Complete results for the interpretation are given in Figure 11. The interpreted data indicate a thin layer of overburden of variable thickness and resistivity. With one exception, its resistivities are in the 25–70 $\Omega \cdot$ m range. Its thickness varies from 0 to 10 m. Fairly uniform resistivities in the

range of 90–360 $\Omega \cdot$ m were obtained for the conductive shale formation. The March sandstone was found to have tenfold greater resistivity, in the 900–3600 $\Omega \cdot$ m range.

The validity of the interpretation was checked by reconstructing the entire anomaly using 2-D numerical modeling. Figure 12 shows one such comparison for the northeast anomaly on line 40 + 50S constructed according to the parameter values shown in Figure 11. The discrepancies between observed and computed tipper magnitudes on the resistive side of the contact and the differences in the two tipper phase profiles on the conductive side of the contact indicate that the contact dips slightly to the northeast. We have also calculated the surface impedances (apparent resistivities) for the model and found that they compare reasonably well with the values observed by Telford et al. (1977). Since there is no confirmed geologic information on the structure responsible for the northeast anomaly, we can only speculate on its origin. The similarity between this feature and the confirmed Gloucester fault suggests a similar origin, such as an uplifted block of older sedimentary rocks similar to those mapped on the southwestern side of the Gloucester fault.

CONCLUSION

The simple method proposed for interpreting the tipper response of subsurface structure allows the analysis of data profiles over the common geologic features of a dipping contact and a buried vertical contact. The charts which relate the observed data characteristics to the parameters of a physical model can be used in the field to interpret single-frequency data profiles. By using only the phase and the shape of the magnitude profile, the effect of the orientation of the target to a fixed source is limited, allowing reasonable interpretation of data related to VLF radio-transmitter sources.

The two examples of the contact interpretation demonstrate that reasonable results can be obtained by this procedure. These examples also show that the interpretation could be improved by increasing the station density in the vicinity of the peak anomaly of the vertical magnetic field. Although this method of interpretation works best when used for the examination of reconnaissance profiles, it can also be used to obtain a starting point for more detailed inversion using other methods.

REFERENCES

Fraser, D. C., 1969, Contouring VLF data: Geophysics, **34**, 958–967.

Jupp, D. L. B., and Vozoff, K., 1977, Two-dimensional magnetotelluric inversion: Geophys. J. Roy. Astr. Soc., **50**, 333–352.

Kaikkonen, P., 1979, Numerical VLF modeling: Geophys. Prosp., **27**, 815–834.

Karous, M., and Hjelt, S. E., 1983, Linear filtering of VLF dip-angle measurements: Geophys. Prosp., **31**, 782–794.

Labson, V. F., Becker, A., Morrison, H. F., and Conti, U., 1985, Geophysical exploration with audiofrequency natural magnetic fields: Geophysics, **50**, 656–664.

Madden, T. R., 1972, Transmission systems and network analogies to geophysical forward and inverse problems: Dept. of Earth and Planetary Sciences, Mass. Inst. of Tech., tech. rep. 72-3.

Morrison, H. F., Lee, K. H., Oppliger, G., and Dey, A., 1979, Magnetotelluric studies in Grass Valley, Nevada: Tech. Rep. LBL-8640, Lawrence Berkeley Lab.

Olsson, O., 1980, VLF anomalies from a perfectly conducting half-plane below an overburden: Geophys. Prosp., **28**, 415–434.

Paterson, N. R., and Ronka, V., 1971, Five years of surveying with the very low frequency electromagnetic method: Geoexplor., **9**, 7–26.

Paul, M. K., and Goodacre, A. K., 1984, The gravity profile and its role in positioning the edge of a two-dimensional faulted structure having an arbitrary vertical variation of density: Geophysics, **49**, 1097–1104.

Ryu, J., 1971, Low frequency electromagnetic scattering: Ph.D. thesis, Univ. of California, Berkeley.

Saydam, A. S., 1981, Very low-frequency electromagnetic interpretation using tilt angle and ellipticity measurements: Geophysics, **46**, 1594–1605.

Telford, W. M., King, W. F., and Becker, A., 1977, VLF mapping of geological structures: Geol. Surv. Can., paper 76-25.

Vozoff, K., 1971, The effect of overburden on vertical component anomalies in AFMAG and VLF exploration: A computer model study: Geophysics, **36**, 53–57.

——— 1972, The magnetotelluric method in exploration of sedimentary basins: Geophysics, **37**, 98–141.

Ward, S. H., 1959, AFMAG—Airborne and ground: Geophysics, **24**, 761–789.

Watts, R. D., 1975, A FORTRAN IV program for analytic continuation of VLF electromagnetic data: U.S. Geol. Surv. open-file rep. 75-159.